Dynamical Analysis of Modal Coupling in Rare-Earth Whispering-Gallery-Mode Microlasers

Jean-Baptiste Ceppe,[1,†] Patrice Féron,[1] Michel Mortier,[2] and Yannick Dumeige[1,*]

[1] *Université de Rennes, CNRS, Institut FOTON – UMR 6082, F-22305 Lannion, France*
[2] *PSL Research University, Chimie ParisTech – CNRS, Institut de Recherche de Chimie de Paris, Paris 75005, France*

(Received 8 March 2019; revised manuscript received 2 May 2019; published 12 June 2019)

We report on an experimental study of a laser regime in erbium-doped whispering-gallery-mode (WGM) microspheres under modal-coupling between the co- and counterpropagating modes. The evidence of modal coupling is observed in the relative intensity noise spectrum of several WGM lasers. Cross-correlation measurements are carried out in order to analyze precisely the emission regimes. It is shown that depending on the material constituting the WGM resonator, frequency-locked bidirectional emission or a self-modulated regime could be reached. The control of the laser emission regime of WGM microlasers is of great importance in the aim of applications in microwave optics or optical sensor miniaturization.

DOI: 10.1103/PhysRevApplied.11.064028

I. INTRODUCTION

Solid-state whispering-gallery-mode (WGM) microcavities combine low mode volume and high quality (Q) factors [1–3]. Therefore, active WGM microcavities made of materials with optical gain can be used as low-threshold lasers [4]. Many WGM lasers [5] have already been investigated: semiconductor microdisks [6–8], silica microtoroids [9], crystalline spheroids [10], and spherical glass microcavities [11] doped with rare-earth ions emitting from visible [12] to mid-infrared [13–15]. These lasers find applications in fundamental physics [16,17], sensing [18–20], optical switching [21], and microwave photonics [22]. Furthermore, rare-earth-doped WGM lasers can reach very narrow linewidth down to 20 kHz in the free running operation [4,23], which gives them many assets for sensing applications [24] or high-purity microwave generation [22]. The WGM laser topologies are similar to those of ring cavity lasers; thus, interesting and complex bidirectional dynamical behavior is expected as is the case for bulk lasers [25–27]. Modal coupling mechanisms in solid-state ring lasers are well understood [28,29]. They have two main contributions: the first is the light reflection or backscattering from optical components, whereas the second is due to population inversion grating [26]. The first coupling tends to favor the existence of co- and counterpropagating waves, while the other one tends toward unidirectional emission. A competition between these two opposite effects can lead to a self-modulation regime depending on their relative strength. Furthermore, Rayleigh backscattering in passive high-finesse WGM microcavities is enhanced, leading to a strong coupling between co- and counterpropagating modes [30–32]. Therefore, bidirectional emission may be privileged in solid-state WGM microlasers. To date, the dynamics and the coupling of co- and counterpropagating modes have been extensively studied in WGM semiconductor lasers [21,33–35]; nevertheless, this effect has been only rarely addressed in the framework of rare-earth WGM lasers [24,36]. In this paper, we report experimental studies on the dynamical behavior of erbium-doped WGM microsphere lasers in which modal coupling occurs. In the first part, we briefly review the different operation regimes of solid-state ring lasers under Rayleigh backscattering. Then, we describe our experimental setup enabling us to measure the relative intensity noise (RIN) and time-domain cross-correlations between the co- and counterpropagating WGM laser signals. Finally, we analyze bidirectional laser emissions from WGM microlasers made of two different host matrices, namely, a phosphate glass (Schott IOG-1 [37]) and a fluoride glass (ZBLALiP [38]), both doped with erbium ions.

II. LASER REGIMES UNDER RAYLEIGH BACKSCATTERING

Figure 1 shows the sketch of a WGM laser consisting of a microsphere coupled to an access waveguide with a rate $1/\tau_P$. The pump field and the laser emissions $s_{\text{out},+}$ and $s_{\text{out},-}$ are respectively inserted in the cavity and extracted

*yannick.dumeige@univ-rennes1.fr
†Present address: Light-Matter Interaction Unit, OIST Graduate University, Onna, Japan.

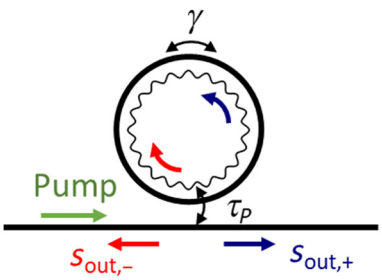

FIG. 1. WGM laser under Rayleigh scattering (coupling rate γ). The interference pattern of the co- and counterpropagating waves leads to a nonuniform gain saturation, which is a nonlinear extra coupling term between the co- and counterpropagating modes. $1/\tau_P$ represents the light-coupling rate from the waveguide to the microcavity.

from the cavity thanks to the access line via an evanescent coupling. The Rayleigh backscattering couples the two counterpropagating modes with a rate γ. Moreover, the interference between these two modes leads to a periodic gain saturation inducing mode coupling by resonant scattering.

The interaction with the gain medium is well described using a semiclassical approach with Maxwell-Bloch equations considering that the electric field can be written as

$$E(z,t) = \mathrm{Re}\left[\tilde{E}_1(t)e^{-j(\omega_0 t - kz)} + \tilde{E}_2 e^{-j(\omega_0 t + kz)}\right], \quad (1)$$

where ω_0 is the mean angular frequency of the emitted signal, z is the curvilinear abscissa along the cavity, k is the the wave vector, $\tilde{E}_1$ is the complex amplitude of the counterclockwise traveling wave ($z > 0$), and $\tilde{E}_2$ is the one traveling in the other direction ($z < 0$). We note that $\tilde{E}_{1,2} = E_{1,2}e^{-j\phi_{1,2}}$, with $E_{1,2} = |\tilde{E}_{1,2}|$. We assume that the laser is single mode and that $\tilde{E}_1$ and $\tilde{E}_2$ have the same polarization. The erbium-doped medium is represented by a three-level system with an excited lifetime $T_1 = 1/A$ (where A is the spontaneous emission rate) and an emission cross section σ. In the case of co- and counterpropagating waves, the two considered fields have the same mode volume and photon lifetime τ_P [31]. N is the refractive index of the cavity and $L = 2\pi a$ is the length of the cavity (which represents also the length of the active medium), where a is the radius of the resonator. As we deal with an erbium-doped medium, the polarization can be adiabatically suppressed and the whole system is described only by the evolution of the electric field amplitudes $E_{1,2}$ and the inverted ion density $\mathcal{N}$. The existence of two lasing modes leads to an interference pattern, modulating the gain medium, as shown in Fig. 1. This diffraction grating induces a supplementary nonlinear coupling. Under the hypothesis of a slightly-above-threshold pumping rate, the whole system is described by

$$\frac{dE_{1,2}}{dt} = -\frac{1}{2\tau_P}E_{1,2} \mp \frac{\gamma}{2}E_{2,1}\sin\left(\Phi + \theta_{1,2}\right) + \frac{c\sigma}{2NL}\oint \mathcal{N}\left[E_{1,2} + E_{2,1}\cos\left(2kz + \Phi\right)\right]dz, \quad (2)$$

$$\frac{d\Phi}{dt} = -\frac{\gamma}{2}\left[\frac{E_2}{E_1}\cos\left(\Phi + \theta_1\right) - \frac{E_1}{E_2}\cos\left(\Phi + \theta_2\right)\right] - \frac{c\sigma}{2NL}\left(\frac{E_1^2 + E_2^2}{E_1E_2}\right)\oint \mathcal{N}\sin\left(2kz + \Phi\right)dz, \quad (3)$$

$$\frac{\partial \mathcal{N}}{\partial t} = \frac{\eta\mathcal{N}_{\mathrm{th}} - \mathcal{N}}{\tau} - \frac{\mathcal{N}}{\tau}\frac{\left|\tilde{E}_1 + \tilde{E}_2\right|^2}{E_{\mathrm{sat}}^2}, \quad (4)$$

where $\Phi = \phi_1 - \phi_2$; $\mathcal{N}_{\mathrm{th}}$ is the inverted ion density at threshold; η is the excitation rate; τ is the recovery time ($\tau^{-1} = W_P + A$, W_P being the pumping rate) [39]; and $\theta_{1,2}$ is the acquired backscattering phase (we assume that θ_1 and θ_2 are close to each other and define $2\delta_\theta = \theta_1 - \theta_2 \ll 1$). One can see in Eq. (2) that γ is a linear coupling term, while $\mathcal{N}$ induces both gain and nonlinear coupling between E_1 and E_2. These two coupling terms, and their relative strength, drive the laser to different regimes. From a stability analysis, it is possible to derive that the laser operates at three different regimes defined by the value of γ [40,41]. Under our hypothesis, the laser exhibits two steady states (unidirectional and bidirectional regimes) and a permanent state (self-modulation). (i) The unidirectional regime is obtained for low values of γ such as $\gamma < (\omega_r/2)$ [40], where ω_r is the relaxation oscillation angular frequency [39]. In this regime, the backscattering is not high enough to authorize the existence of two traveling modes and the mode with higher amplitude gets the higher gain [42]. (ii) The self-modulated regime is obtained for intermediate values of γ. This is a periodic permanent regime in which the two lasing modes are antiphase oscillating at the angular frequency γ [26,40,43]. The modulation contrast $\mathcal{C}$ decreases with γ as follows:

$$\mathcal{C} = \sqrt{1 - \left(\frac{2\gamma\,|\delta_\theta|\,\tau_P'}{\eta - 1 - \gamma\,|\delta_\theta|\,\tau_P'}\right)^2}, \quad (5)$$

with $\tau_P'^{-1} = \tau_P^{-1} - \gamma\,|\delta_\theta|$. When $\mathcal{C}$ reaches zero, the laser shows a bidirectional behavior. (iii) This bidirectional regime is obtained for high values of γ [40,44]:

$$\gamma > \frac{1}{\tau_P\,|\delta_\theta|}\left(\frac{\eta - 1}{\eta + 2}\right). \quad (6)$$

In this case, the two traveling waves are automatically frequency locked together [39], which is the main problem for solid-state ring laser gyroscopes [25].

III. EXPERIMENTS

A. Setup description

We have two glasses with different host matrices at our disposal: IOG-1 an industrial phosphate glass from Schott and ZBLALiP a fluoride glass. Both glasses are doped with erbium ions (3.25×10^{20} ions/cm^3 for IOG-1 and 0.2×10^{20} ions/cm^3 for ZBLALiP). Microspheres are manufactured by a melting technique from a glass powder using a plasma torch [38]. This process enables us to make microspheres with diameters $2a$ between 60 and 150 μm. Figure 2 shows the experimental setup used to analyze the laser emission of our microcavities. The erbium transition ${}^4I_{13/2} \rightarrow {}^4I_{15/2}$ is excited using a 1480-nm laser diode (pump laser) whose maximal power is 100 mW. We use a tapered fiber, whose diameter is reduced to about 1 μm, to couple the pump into the microcavity. The co- and counterpropagating signals are collected using the same tapered fiber [11,45]. $s_{\text{out},-}$ is separated from the initial pump with a wavelength demultiplexer. The laser emissions of interest are then optically filtered using manually tunable optical filters (Yenista XTM-50, bandwidth 4 GHz). RIN measurements are performed on both emission directions using a photodetection system already reported in previous work [45] and depicted in Fig. 2. The low-noise transimpedance amplifier (Femto DHPCA-100) converts the photocurrents into voltages V_1 and V_2. Electrical filters (Thorlabs EF500, cutoff frequency 1 Hz) are used to suppress the dc component of the two voltages. Power spectrum density of the noise is measured using an electrical spectrum analyzer (ESA) (Agilent, bandwidth: 40 MHz). The whole photodetecting chain is well suited to RIN measuring up to 10–20 MHz. By replacing the ESA by an oscilloscope (Wavemaster LeCroy), we can also perform the photodetection in the time domain and thus infer cross-correlations between the counterpropagating laser emissions using the following procedure. First, voltages V_1 and V_2 are normalized as follows:

$$x(t) = \frac{V_1(t) - \langle V_1 \rangle}{\sigma_{V_1}}, \tag{7}$$

$$y(t) = \frac{V_2(t) - \langle V_2 \rangle}{\sigma_{V_2}}, \tag{8}$$

where $\langle \cdot \rangle$ is the temporal average and $\sigma_{V_{1,2}}$ the standard deviation of $V_{1,2}$. We then calculate the cross-correlation function Γ_{xy} and the autocorrelation functions Γ_{xx} and Γ_{yy}, defined by

$$\Gamma_{xy}(\tau) = \langle x(t)y(t-\tau) \rangle, \tag{9}$$

$$\Gamma_{xx}(\tau) = \langle x(t)x(t-\tau) \rangle, \tag{10}$$

$$\Gamma_{yy}(\tau) = \langle y(t)y(t-\tau) \rangle. \tag{11}$$

Finally, we obtain the normalized cross-correlation function

$$\Theta_{xy}(\tau) = \frac{\Gamma_{xy}(\tau)}{\sqrt{\Gamma_{xx}(0)\Gamma_{yy}(0)}}. \tag{12}$$

B. Experimental results in IOG-1 glass

We first use an IOG-1 microsphere with a diameter of 105 μm. The optical filters are both centered on the laser emission wavelength, which is the same for both propagation directions (1564 nm). After filtering, the photodetected powers are 150 nW for $s_{\text{out},+}$ and 86 nW for $s_{\text{out},-}$. RIN spectra for co- and counterpropagating modes are presented in Fig. 3(a). These spectra show one peak at the relaxation oscillation frequency, which is the signature of a class-B laser operation and also some associated harmonic frequencies due to the low mode volume of the cavity [45]. The RIN spectra of the two counterpropagating modes are similar; in particular, they have the same relaxation oscillation frequencies ($\omega_r/2\pi = 257$ kHz), which shows that the two modes have the same photon lifetimes and pumping rates. Furthermore, since the relative intensities of the harmonic and fundamental peaks are the same, the two counterpropagating modes have the same mode volume [45]. Therefore, we can conclude that the WGM $s_{\text{out},+}$ and $s_{\text{out},-}$ have the same radial (n) and orbital (ℓ) orders and opposite azimutal (m) order since they propagate in opposite directions. There is also an

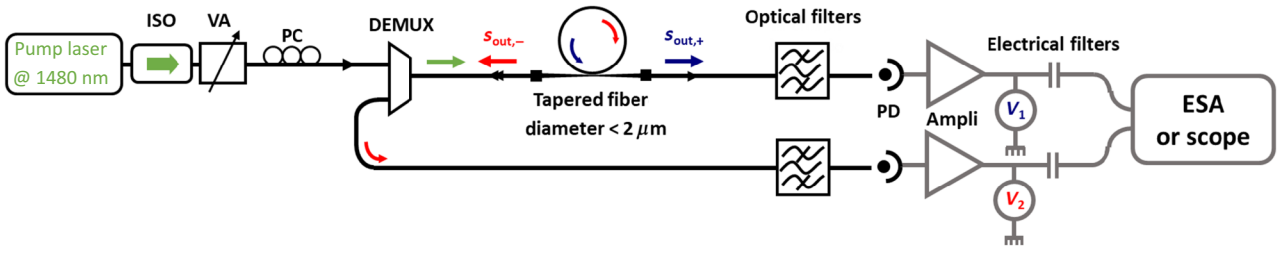

FIG. 2. Experimental setup: ISO, optical isolator; VA, variable attenuator; PC, polarization controller; DEMUX, wavelength demultiplexer; PD, photodiodes; Ampli, transimpedance amplifiers; Optical filter, narrow band-pass optical filters; Electrical filters, dc block filters or high-pass filters; ESA, electrical spectrum analyzer. The ESA is used to measure the RIN in the frequency domain, whereas the oscilloscope is used for cross-correlation measurements in the time domain.

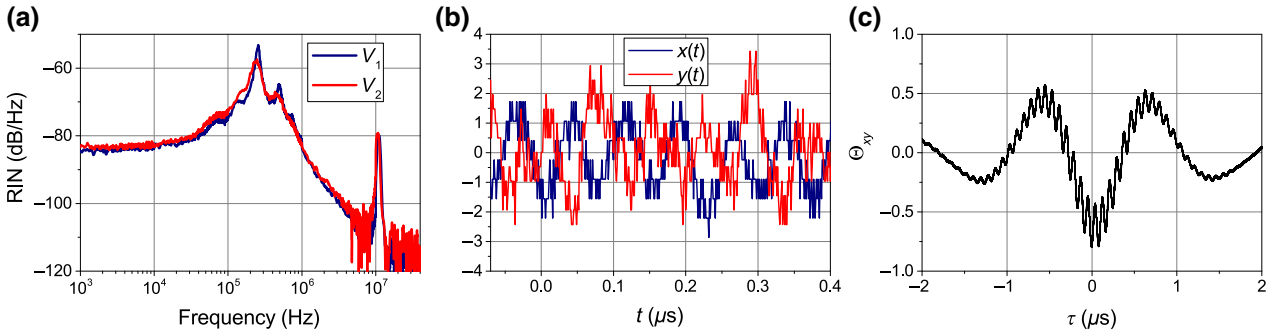

FIG. 3. Experimental results obtained in a 105-μm diameter IOG-1 microsphere. (a) RIN spectrum for the co- and counterpropagating emitted modes. (b) Time-domain series $x(t)$ and $y(t)$ obtained from centering and normalization of $V_1(t)$ and $V_2(t)$. (c) Normalized cross-correlation function.

additional RIN peak at 12 MHz. This RIN peak can result from the self-modulation behavior of the WGM laser submitted to modal coupling owing to Rayleigh backscattering as recalled in Sec. II. To confirm this hypothesis, we also perform cross-correlation measurements following the procedure presented in Sec. III A. As we are only interested in high frequencies (higher than the relaxation oscillation frequency), and because of the high intrinsic noise level of the laser itself, we use an electrical high-pass filter with a cutoff frequency of 600 kHz (Thorlabs EF517). Normalized voltages $x(t)$ and $y(t)$ and the cross-correlation function $\Theta_{xy}(\tau)$ are presented in Figs. 3(b) and 3(c). The phase opposition between $x(t)$ and $y(t)$, clearly seen in Fig. 3(b), leads to a strong anticorrelation, highlighted by the value of the cross-correlation for short times $\Theta_{xy}(\tau = 0) = -0.8$. This confirms the hypothesis of self-modulation operation of our IOG-1 WGM laser due to the competition between Rayleigh backscattering and gain saturation (see Sec. II). The overmodulation with a long period (corresponding to the third harmonic of the relaxation oscillation frequency) appearing in $\Theta_{xy}(\tau)$ comes from an excess of intrinsic noise that has not been suppressed by the electrical filtering. Note that the cross-correlation function associated to this modulation, given by the envelope of the curve shown in Fig. 3(c), has a strong negative value for short delays as well.

C. Experimental results in ZBLALiP glass

We also tested a ZBLALiP microsphere with a diameter of 100 μm. After optical filtering at 1558 nm, the photodetected powers are 157 nW for $s_{\text{out},+}$ and 27 nW for $s_{\text{out},-}$. We can thus deduce that the laser operates either in the self-modulated regime (ii) or in the bidirectional regime (iii). We observe two relaxation oscillation frequencies in the RIN spectra due to the fact that for a given emission direction, the WGM microsphere has now two modes with different quantum numbers propagating in the same direction. Nevertheless, the two RIN spectra for the two opposite propagation directions perfectly match and, thus, the signals emitted in both directions correspond to the same WGM. As our RIN measurement setup is limited to frequencies smaller than 40 MHz, we cannot determine precisely if the laser operates in regimes (ii) or (iii), since the beating frequency could appear at higher frequencies. Cross-correlation measurements are also performed using a dc block electrical filter. Normalized voltages $x(t)$ and $y(t)$ and normalized cross-correlation function $\Theta_{xy}(\tau)$ are presented in Figs. 4(b) and 4(c). Now, we observe a perfect correlation between the co- and counterpropagating signals. Under the assumption that the correlations between the two counterpropagating signals persist at the relaxation oscillation frequency and its harmonics (see Sec. III B), we might conclude that the lasers operate in the bidirectional regime.

D. Discussion

The two studied WGM lasers emit light in both directions but may operate in two different regimes. The IOG-1 laser for which the co- and counterpropagating modes are emitted in antiphase operates in a self-modulation regime at $\gamma/2\pi = 12$ MHz and could be used as a miniaturized laser gyroscope. In contrast, the fluoride glass WGM laser does not show a beat note up to 40 MHz, which is the cutoff frequency of our measurement chain. This laser either operates in the bidirectional regime and thus could not be used for laser gyroscope applications or in the self-modulated regime with a high coupling rate γ. Assuming that 40 MHz corresponds to the limit given by Eq. (6), we can deduce that if operating in regime (ii) as a laser gyroscope, the minimum blind region $\Omega_{B,\min}$ of the fluoride glass microlaser is given by [44,46,47]

$$\Omega_{B,\min} \approx \gamma\,|\delta_\theta| = \frac{1}{\tau_P}\frac{\eta-1}{\eta+2}. \tag{13}$$

The fit of the RIN spectrum [45] given in Fig. 4(a) (V_1) enables us to determine $\eta = 66$ and $\tau_P = 66.7$ ns, which gives $\Omega_{B,\min} = 15 \times 10^6$ rad/s. Assuming comparable values of δ_θ for the two WGM lasers, the blind region of the

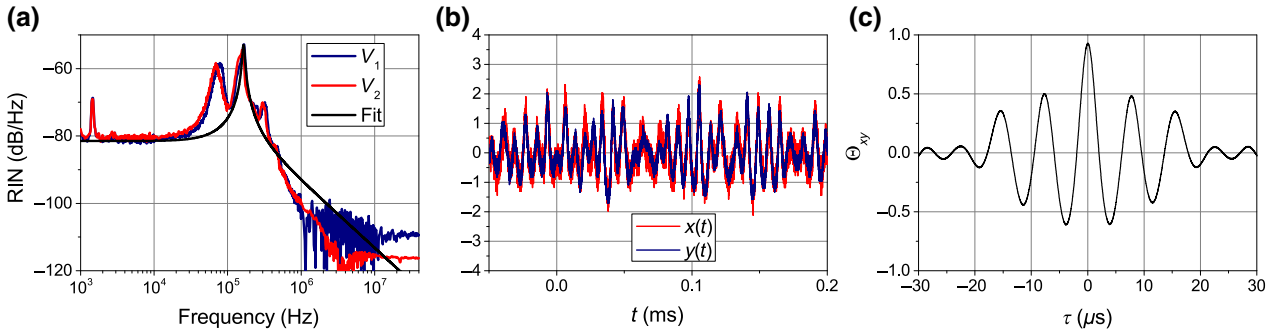

FIG. 4. Experimental results obtained in a 100-μm-diameter ZBLALiP microsphere. (a) RIN spectrum for the co- and counterpropagating emitted modes. The fit is made using the model given in Ref. [45] considering only the mode with the highest RIN and neglecting the relaxation frequency harmonics. The peak at 1.5 kHz comes from parasitic noises. (b) Time-domain series $x(t)$ and $y(t)$ obtained from centering and normalization of $V_1(t)$ and $V_2(t)$. (c) Normalized cross-correlation function.

IOG-1 laser would be less than 4.5×10^6 rad/s. Consequently, in any case, the fluoride glass is less well suited for WGM laser gyroscope applications than the IOG-1 glass.

Inspection of Eq. (6) reveals that one of the key parameters determining the laser operation is the linear coupling rate between the two counterpropagating modes. Assuming that photon lifetimes and pumping rates are comparable, we can deduce from the previous experiments that the linear coupling strength is much stronger for ZBLALiP than for IOG-1 glass. This can be confirmed by linear optical transmission measurements. This process consists of using a tunable narrow-band laser ($\leq$ 150 kHz) frequency-swept across the WGM resonance and simultaneously recording the transmission [38,48]. A thorough frequency calibration allows us to obtain the linear transmission spectrum. We give such measurements done for our two glasses in Fig. 5. Note that these spectra are obtained with other microspheres made of the same materials as those used in laser experiments. Nevertheless, it informs us about the typical frequency splitting $2\delta_C \approx \gamma/2\pi$ [32], which can be reached both for IOG-1 and ZBLALiP WGM microspheres. For IOG-1, the frequency splitting is such that $2\delta_C = 23$ MHz, whereas for ZBLALiP it is around 390 MHz. This confirms that the Rayleigh backscattering is much stronger in the fluoride glass than in the phosphate glass. Moreover, the frequency splitting obtained for IOG-1 WGM resonators is comparable to the beating frequency (12 MHz) measured in the RIN when the self-modulation operation is reached. Finally, we can note that, in both cases, the coupling rate is much larger than the relaxation oscillation frequency, which supports the fact that these WGM lasers do not operate in the unidirectional regime.

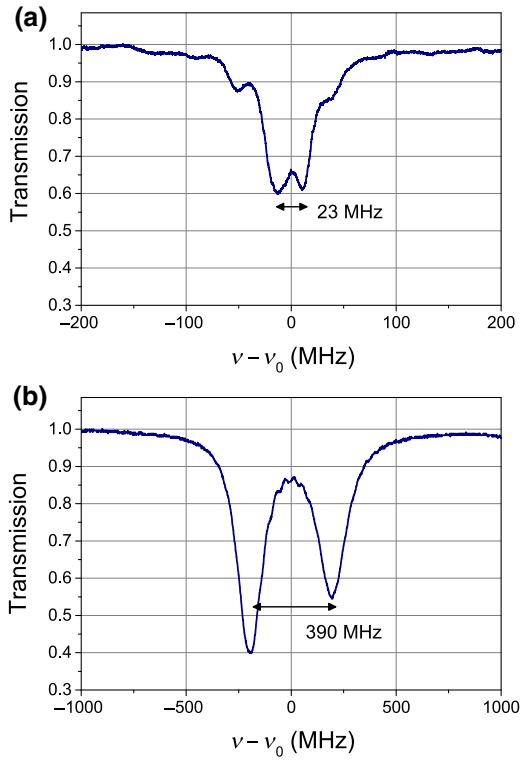

FIG. 5. Typical linear transmission spectrum measured for (a) an IOG-1 microsphere under the laser threshold and (b) a ZBLALiP passive (without erbium doping) microsphere. ν is the frequency of the probe laser and ν_0 is the resonance frequency of the WGM microsphere.

IV. CONCLUSION

We simultaneously measure the RIN spectra of the two counterpropagating signals emitted by erbium-doped WGM class-B microlasers. In addition to noise peaks at the relaxation oscillation frequency and its harmonics, the analysis of the RIN spectrum of phosphate glass microspherical laser reveals an extra peak due to the self-modulation operation induced by a Rayleigh-backscattering-induced modal coupling. Cross-correlation measurements between the co- and counterpropagating laser signals show a neat antiphase oscillation confirming

the self-modulation regime [45]. We repeat this measurement using a fluoride glass WGM laser and, in this case, we do not observe any beat note up to 40 MHz. This can be interpreted as a laser operating in the bidirectional regime or in a self-modulated regime with a high modulation frequency. This behavior difference is well supported by the fact that Rayleigh backscattering is much stronger in our fluoride glass microspheres than in phosphate glass microcavities. Controlling the bidirectional feature of miniaturized WGM lasers is crucial for applications. For instance, integrated laser gyroscopes must operate in the self-modulation regime [26]. Furthermore, a good knowledge of the physical and optical properties of materials would be of importance to properly design the microlaser gyroscope. When the modal coupling rate is experimentally determined, the photon lifetime, which can be controlled via the evanescent coupling with the access line, can be adapted to reach the self-modulation regime using Eq. (6). Conversely, for all-optical compact microwave sources, a bidirectional behavior is preferred since it would avoid the apparition of spurious spikes in the rf spectrum.

ACKNOWLEDGMENTS

J.-B.C. thanks the Centre National d'Études Spatiales (CNES) and Région Bretagne (ARED) for financial support. Y.D. is a member of the Institut Universitaire de France. The authors acknowledge fruitful discussions with S. Trebaol.

[1] K. J. Vahala, Optical microcavities, Nature **424**, 839 (2003).
[2] V. S. Ilchenko and A. B. Matsko, Optical resonators with whispering-gallery modes-part II: Applications, IEEE J. Sel. Topics Quantum Electron. **12**, 15 (2006).
[3] A. Chiasera, Y. Dumeige, P. Féron, M. Ferrari, Y. Jestin, G. Nunzi Conti, S. Pelli, S. Soria, and G. Righini, Spherical whispering-gallery-mode microresonators, Laser Photonics Rev. **4**, 457 (2010).
[4] V. Sandoghdar, F. Treussart, J. Hare, V. Lefèvre-Seguin, J. M. Raimond, and S. Haroche, Very low threshold whispering-gallery-mode microsphere laser, Phys. Rev. A **54**, R1777 (1996).
[5] L. He, A. K. Özdemir, and L. Yang, Whispering gallery microcavity lasers, Laser Photonics Rev. **7**, 60 (2013).
[6] S. L. McCall, A. F. J. Levi, R. E. Slusher, S. J. Pearton, and R. A. Logan, Whispering–gallery mode microdisk lasers, Appl. Phys. Lett. **60**, 289 (1992).
[7] Y. Zhang, X. Zhang, K. H. Li, Y. F. Cheung, C. Feng, and H. W. Choi, Advances in III-nitride semiconductor microdisk lasers, Phys. Status Solidi A **212**, 960 (2015).
[8] A. Elbaz, M. El Kurdi, A. Aassime, S. Sauvage, X. Checoury, I. Sagnes, C. Baudot, F. Boeuf, and P. Boucaud, Germanium microlasers on metallic pedestals, APL Photonics **3**, 106102 (2018).
[9] E. P. Ostby, L. Yang, and K. J. Vahala, Ultralow-threshold Yb^{3+}:SiO_2 glass laser fabricated by the solgel process, Opt. Lett. **32**, 2650 (2007).
[10] S. J. Herr, C. S. Werner, K. Buse, and I. Breunig, Quasi-phase-matched self-pumped optical parametric oscillation in a micro-resonator, Opt. Express **26**, 10813 (2018).
[11] F. Lissillour, D. Messager, G. Stéphan, and P. Féron, Whispering-gallery-mode laser at 1.56 μm excited by a fiber taper, Opt. Lett. **26**, 1051 (2001).
[12] F. Tabataba-Vakili, L. Doyennette, C. Brimont, T. Guillet, S. Rennesson, E. Frayssinet, B. Damilano, J.-Y. Duboz, F. Semond, I. Roland, M. El Kurdi, X. Checoury, S. Sauvage, B. Gayral, and P. Boucaud, Blue microlasers integrated on a photonic platform on silicon, ACS Photonics **5**, 3643 (2018).
[13] G. Palma, M. C. Falconi, F. Starecki, V. Nazabal, T. Yano, T. Kishi, T. Kumagai, and F. Prudenzano, Novel double step approach for optical sensing via microsphere WGM resonance, Opt. Express **24**, 26956 (2016).
[14] G. Palma, M. C. Falconi, F. Starecki, V. Nazabal, J. Ari, L. Bodiou, J. Charrier, Y. Dumeige, E. Baudet, and F. Prudenzano, Design of praseodymium-doped chalcogenide micro-disk emitting at 4.7 μm, Opt. Express **25**, 7014 (2017).
[15] B. Behzadi, R. K. Jain, and M. Hossein-Zadeh, Spectral and modal properties of a mid-IR spherical microlaser, IEEE J. Quantum Electron. **53**, 1 (2017).
[16] J. M. Gerard and B. Gayral, Strong purcell effect for InAs quantum boxes in three-dimensional solid-state microcavities, J. Lightwave Technol. **17**, 2089 (1999).
[17] V. Huet, A. Rasoloniaina, P. Guillemé, P. Rochard, P. Féron, M. Mortier, A. Levenson, K. Bencheikh, A. Yacomotti, and Y. Dumeige, Millisecond Photon Lifetime in a Slow-light Microcavity, Phys. Rev. Lett. **116**, 133902 (2016).
[18] C. Ciminelli, F. Dell'Olio, C. E. Campanella, and M. N. Armenise, Photonic technologies for angular velocity sensing, Adv. Opt. Photonics **2**, 370 (2010).
[19] J. Ward and O. Benson, WGM microresonators: Sensing, lasing and fundamental optics with microspheres, Laser Photonics Rev. **5**, 553 (2011).
[20] J. Ren, H. Hodaei, G. Harari, A. U. Hassan, W. Chow, M. Soltani, D. Christodoulides, and M. Khajavikhan, Ultrasensitive micro-scale parity-time-symmetric ring laser gyroscope, Opt. Lett. **42**, 1556 (2017).
[21] L. Liu, R. Kumar, K. Huybrechts, T. Spuesens, G. Roelkens, E.-J. Geluk, T. de Vries, P. Regreny, D. van Thourhout, R. Baets, and G. Morthier, An ultra-small, low-power, all-optical flip-flop memory on a silicon chip, Nat. Photonics **4**, 182 (2010).
[22] L. Xiao, S. Trebaol, Y. Dumeige, Z. Cai, M. Mortier, and P. Feron, Miniaturized optical microwave source using a dual-wavelength whispering gallery mode laser, IEEE Photonics Technol. Lett. **22**, 559 (2010).
[23] F. Lissillour, R. Gabet, P. Féron, P. Besnard, and G. Stéphan, Linewidth narrowing of a DFB semiconductor laser at 1.55 μm by optical injection of an Er:ZBLAN microspherical laser, EPL (Europhys. Lett.) **55**, 499 (2001).
[24] L. He, S. K. Ozdemir, Y. F. Xiao, and L. Yang, Gain-induced evolution of mode splitting spectra in a high-Q active microresonator, IEEE J. Quantum Electron. **46**, 1626 (2010).

[25] S. Schwartz, G. Feugnet, P. Bouyer, E. Lariontsev, A. Aspect, and J.-P. Pocholle, Mode-coupling Control in Resonant Devices: Application to Solid-State Ring Lasers, Phys. Rev. Lett. **97**, 093902 (2006).

[26] S. Schwartz, G. Feugnet, E. Lariontsev, and J.-P. Pocholle, Oscillation regimes of a solid-state ring laser with active beat-note stabilization: From a chaotic device to a ring-laser gyroscope, Phys. Rev. A **76**, 023807 (2007).

[27] S. Schwartz, F. Gutty, G. Feugnet, P. Bouyer, and J.-P. Pocholle, Suppression of Nonlinear Interactions in Resonant Macroscopic Quantum Devices: The Example of the Solid-State Ring Laser Gyroscope, Phys. Rev. Lett. **100**, 183901 (2008).

[28] I. Efanova and E. Lariontsev, Interaction of oppositely directed waves in a solid state ring laser, Soviet Phys. JETP **28**, 802 (1968).

[29] P. A. Khandokhin and Y. I. Khanin, Instabilities in a solid-state ring laser, J. Opt. Soc. Am. B **2**, 226 (1985).

[30] D. Weiss, V. Sandoghdar, J. Hare, V. Lefevre-Seguin, J.-M. Raimond, and S. Haroche, Splitting of high-Q Mie modes induced by light backscattering in silica microspheres, Opt. Lett. **20**, 1835 (1995).

[31] T. J. Kippenberg, A. L. Tchebotareva, J. Kalkman, A. Polman, and K. J. Vahala, Purcell-factor-enhanced Scattering from Si Nanocrystals in an Optical Microcavity, Phys. Rev. Lett. **103**, 027406 (2009).

[32] S. Trebaol, Y. Dumeige, and P. Féron, Ringing phenomenon in coupled cavities: Application to modal coupling in Whispering-Gallery-Mode resonators, Phys. Rev. A **81**, 043828 (2010).

[33] M. Sorel, G. Giuliani, A. Scire, R. Miglierina, S. Donati, and P. J. R. Laybourn, Operating regimes of GaAs-AlGaAs semiconductor ring lasers: experiment and model, IEEE J. Quantum Electron. **39**, 1187 (2003).

[34] G. Giuliani, R. Miglierina, M. Sorel, and A. Scire, Linewidth, autocorrelation, and cross-correlation measurements of counterpropagating modes in GaAs-AlGaAs semiconductor ring lasers, IEEE J. Sel. Topics Quantum Electron. **11**, 1187 (2005).

[35] J. Javaloyes and S. Balle, Emission directionality of semiconductor ring lasers: A traveling-wave description, IEEE J. Quantum Electron. **45**, 431 (2009).

[36] L. He, S. K. Özdemir, J. Zhu, and L. Yang, Ultrasensitive detection of mode splitting in active optical microcavities, Phys. Rev. A **82**, 053810 (2010).

[37] D. Ristić, S. Berneschi, M. Camerini, D. Farnesi, S. Pelli, C. Trono, A. Chiappini, A. Chiasera, M. Ferrari, A. Lukowiak, Y. Dumeige, P. Féron, G. Righini, S. Soria, and G. N. Conti, Photoluminescence and lasing in whispering gallery mode glass microspherical resonators, J. Lumin. **170**, 755 (2016).

[38] A. Rasoloniaina, V. Huet, T. K. N. Nguyên, E. L. Cren, M. Mortier, L. Michely, Y. Dumeige, and P. Féron, Controling the coupling properties of active ultrahigh-Q WGM microcavities from undercoupling to selective amplification, Sci. Rep. **4**, 4023 (2014).

[39] A. E. Siegman, *Lasers* (University Science Books, Mill Valley, Calif, 1986).

[40] N. V. Kravtsov and E. G. Lariontsev, Nonlinear dynamics of solid-state ring lasers, Quantum Electron. **36**, 192 (2006).

[41] S. Schwartz, Thèse de doctorat, Ecole Polytechnique X (2006).

[42] G. Perevedentseva, P. A. Khandokhin, and Y. I. Khanin, Theory of a single-frequency solid-state ring laser, Soviet J. Quantum Electron. **10**, 71 (1980).

[43] E. L. Klochan, L. S. Kornienko, N. V. Kravtsov, E. G. Lariontsev, and A. N. Shelaev, Oscillation regimes in a rotating solid-state ring laser, JETP **38**, 669 (1974).

[44] J.-B. Ceppe, Thèse de doctorat, Université de Rennes 1 (2018).

[45] J.-B. Ceppe, M. Mortier, P. Féron, and Y. Dumeige, Theoretical and experimental analysis of rare earth whispering gallery mode laser relative intensity noise, Opt. Express **25**, 32732 (2017).

[46] R. Adler, A study of locking phenomena in oscillators, Proc. IRE **34**, 351 (1946).

[47] W. W. Chow, J. Gea-Banacloche, L. M. Pedrotti, V. E. Sanders, W. Schleich, and M. O. Scully, The ring laser gyro, Rev. Mod. Phys. **57**, 61 (1985).

[48] Y. Dumeige, S. Trebaol, L. Ghişa, T. K. N. Nguyên, H. Tavernier, and P. Féron, Determination of coupling regime of high-Q resonators and optical gain of highly selective amplifiers, J. Opt. Soc. Am. B **25**, 2073 (2008).